International Journal of Nanomedicine

Dovepress
open access to scientific and medical research

Open Access Full Text Article

ORIGINAL RESEARCH

Biocompatibility evaluation of antibacterial Ti–Ag alloys with nanotubular coatings

This article was published in the following Dove Medical Press journal:
International Journal of Nanomedicine

Xingwang Liu,[1,2,*] Chen Chen,[3,*] Hangzhou Zhang,[4] Ang Tian,[5] Junhua You,[6] Lin Wu,[7] Zeming Lei,[8] Xi Li,[8] Xizhuang Bai,[8] Shiyi Chen[1]

[1]Department of Sports Medicine, Huashan Hospital of Fudan University, Shanghai 200040, China; [2]State Key Laboratory of Molecular Engineering of Polymers, Fudan University, Shanghai 200082, China; [3]Department of Arthroscopic Surgery, Shanghai Jiao Tong University Affiliated Sixth People's Hospital, Shanghai 200233, China; [4]Department of Sports Medicine and Joint Surgery, The First Affiliated Hospital of China Medical University, Shenyang 110000, China; [5]Liaoning Provincial Key Laboratory of Metallurgical Resources Circulation Science, Northeastern University, Shenyang 110819, China; [6]School of Materials Science and Engineering, Shenyang University of Technology, Shenyang 110870, China; [7]Department of Prosthodontics, School of Stomatology, China Medical University, Shenyang 110000, China; [8]Department of Orthopaedics, The People's Hospital of China Medical University, Shenyang 110000, China

*These authors contributed equally to this work

Background: Implant-related infection is a major problem postsurgery. As an alternative to a localized antibiotic release system, we used Ag to fabricate Ti–Ag alloys with nanotubular coatings (TiAg-NTs). Ag has excellent antibacterial properties, but its biological toxicity is a concern. Therefore, we performed biological experiments both in vitro and in vivo to evaluate the biocompatibility of TiAg-NTs with different concentrations of Ag (1%, 2%, and 4%).

Methods: For in vitro experiments, cytocompatibility, including cell attachment, viability, and proliferation, was tested, and genes and proteins related to osteogenic differentiation were also evaluated. For in vivo assays, the rat femoral condylar insertion model was used, and micro-computed tomography (micro-CT) and histological analysis were conducted to analyze bone formation around implants at 1, 2, and 4 weeks after surgery.

Results: Both in vitro and in vivo results indicate that Ti2%Ag-NT showed comparable cytocompatibility with commercially pure Ti (cp-Ti), and it could achieve good osseointegration with the surrounding bone tissue.

Conclusion: We thus believe that Ti2%Ag-NT is a potential biomaterial for orthopedics.

Keywords: Ag, Ti, alloy, nanotube, biocompatibility

Introduction

Implants are foreign materials in the human body, and they are a preferential site for bacterial adhesion, which may lead to implant-related infection (IRI).[1] Once IRI occurs, patients have to undergo debridement and implant removal surgery, prolonged and high-dose antibiotic treatment, and eventually a revision surgery, which is a substantial burden for both patients and society.

Ag is a well-recognized and highly effective antibacterial agent that can kill a broad spectrum of bacteria and remain stable under physiological conditions.[2] The ability of Ag ions to prevent biofilm formation on the surface of biomaterials has been confirmed.[3] Compared to traditional localized antibiotic delivery systems,[4] Ag-containing biomaterials have three advantages. First, the initial burst release and subsequent local toxicity are relatively low.[5] Second, the late-phase persistent low-level release and consequent bacterial resistance are alleviated.[6] Third, all organic antibiotics, such as vancomycin, have a shelf life and are denatured in vivo after a long period of time, which makes it impossible to achieve long-term antibacterial effects. Therefore, Ag ions are more desirable long-term antibacterial agents than organic antibiotics. However, the biological toxicity of Ag ions remains a challenge.

Nanotube (NT) arrays have been considered to be an effective means of improving the biocompatibility of metal implants for their unique properties.[7] First, the preparation of NTs on metal surfaces is highly cost-effective.[8] Second, the nanoroughness of the implant surface mimics the nanomorphology of bone and promotes the interaction

Correspondence: Shiyi Chen
Department of Sports Medicine, Huashan Hospital of Fudan University, Shanghai 200040, China
Tel +86 21 5241 2249
Fax +86 21 5241 3903
Email cshiyi@163.com

Xizhuang Bai
Department of Orthopaedics, The People's Hospital of China Medical University, No. 33 Wenyi Road, Shenhe District, Shenyang 110000, China
Tel +86 135 0490 0218
Fax +86 24 2401 6595
Email doctor_baixizhuang@163.com

submit your manuscript | www.dovepress.com
Dovepress
http://dx.doi.org/10.2147/IJN.S193569

between the implant and adjacent cells, thereby promoting initial osseointegration and binding strength.[9] Third, nanotube arrays have a hydrophilic surface that promotes initial cell adhesion, and the connecting channels between nanotube walls provide a space for the exchange of nutrients and gas.[10] In addition, NTs have a high surface area and are a natural reservoir for drugs. NT diameter, length, and other parameters can be easily changed to modulate their biological behavior.[11]

In our previous study,[12] we reported the fabrication of Ti–Ag alloys with nanotubular coatings (TiAg-NTs, 1%, 2%, and 4%). The difference between TiAg-NTs and other Ag-containing biomaterials mainly includes the following: first, this study sintered Ag and Ti together in their entirety instead of using the postloading technique.[13–15] Second, TiAg-NTs exert biological effects by releasing Ag ions instead of Ag nanoparticles.[16] This preparation method firmly fixes Ag to the surface of the material, which not only avoids the potential hazard of free nanoparticles but also facilitates long-term antibacterial properties. Furthermore, excellent antibacterial properties, satisfactory cell viability, and a low cellular apoptosis rate were observed from Ti2%Ag-NT. However, these experiments only provided a good start, and we need to conduct more comprehensive experiments to demonstrate the biocompatibility of Ti2%Ag-NT and other TiAg-NTs, especially the experiments in vivo. Implanting the biomaterial into bone to verify its osseointegration property is a more powerful support for its future medical application. In addition, environmental cues such as the bone marrow environment, mechanical stimulation conducted by bone, and continuous exchange of the liquids around implants may cause discrepancies between in vitro and in vivo experiments. Therefore, in this study, the biocompatibility of TiAg-NTs was tested both in vitro and in vivo with commercially pure Ti (cp-Ti) as a control.

Materials and methods

Nanotube fabrication

Samples with dimensions of Φ14×2 mm^3 and Φ1×15 mm^3 were used as substrates for in vitro and in vivo tests (Figures 1 and 2). As previously reported,[12] cp-Ti and Ti–Ag sintered alloy samples (1, 2, and 4 wt% Ag) were polished and washed in acetone and ultrasonically cleaned for 30 minutes. The samples were washed three times with deionized water and then dried under a stream of nitrogen gas. A two-step anodization process was then applied to fabricate the nanotubes. During this process, the samples were first anodized under a constant voltage of 60 V for 2 hours in an ethanediol solution containing 0.5 wt% ammonium fluoride, cleaned in hydrochloric acid, dried with nitrogen gas, and then anodized under a constant voltage of 20 V for 4 hours. Platinum slices were used as a counter electrode. The nanotube coatings were then thermally treated at 450°C in air to obtain a stable crystal phase.

Biocompatibility assays in vitro

Cell culture

The MG63 cell line (The Cell Bank of Type Culture Collection of Chinese Academy of Sciences, Shanghai, China)

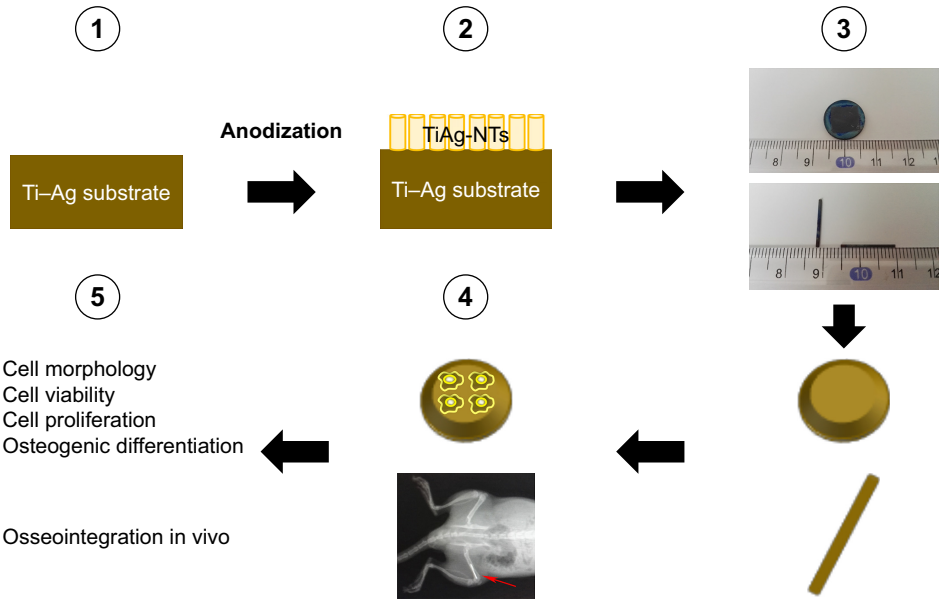

Figure 1 A schematic showing fabrication steps of Ti–Ag alloys with nanotubular coatings and its cellular responses as well as osseointegrative properties.
Abbreviation: NT, nanotube.

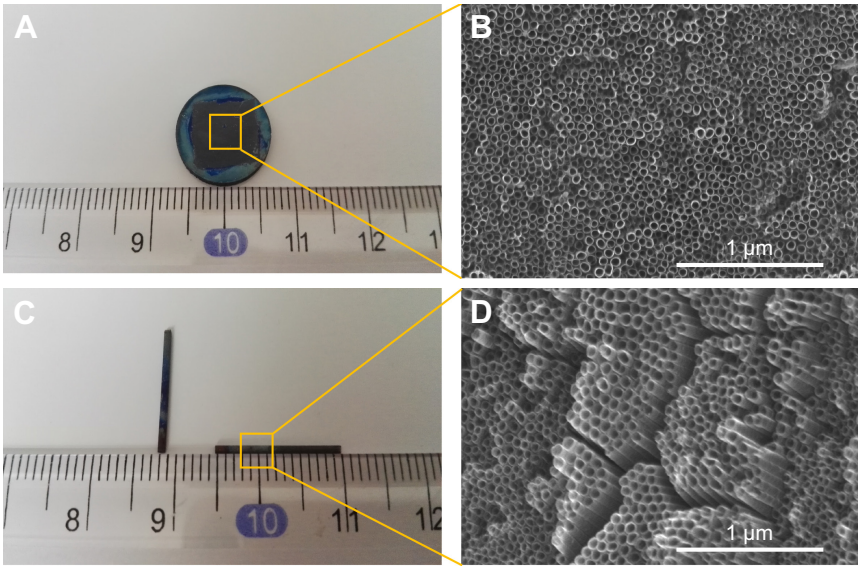

Figure 2 (**A** and **C**) Macroscopic images of Ti2%Ag-NT used in vitro and in vivo. (**B** and **D**) SEM images of nanotubes formed on the surface of Ti2%Ag-NT.
Abbreviations: NT, nanotubes; SEM, scanning electron microscope.

was used for the biocompatibility assays. The cells were cultured in high-glucose DMEM (Thermo Fisher Scientific, Waltham, MA, USA) with 10% FBS (PAN Biotech GmbH, Berlin, Germany) and 1% penicillin–streptomycin (Thermo Fisher Scientific) under standard culture conditions (95% humidity, 5% CO_2, and 37°C). The culture medium was changed every other day, and the cells were passaged once they reached 80% confluence.[12]

Morphology

The samples were placed at the bottom of a 24-well plate, and 1 mL of MG63 cell suspension (1×10^5 cells/mL) was seeded onto each sample. After culturing for 1 day under standard culture conditions, samples were washed twice with PBS and then fixed with 2.5% glutaraldehyde (Solarbio Company, Beijing, China) for 2 hours at 4°C. After stepwise dehydration of the samples with serial concentrations of ethanol for 10 minutes at each concentration (50%, 60%, 70%, 80%, 90%, 95%, and 100%), the samples were critical-point dried and coated with Au for imaging with scanning electron microscope (SEM, SU8010; Hitachi Ltd., Tokyo, Japan).[17]

Viability

A Live and Dead Viability/Cytotoxicity Assay (KeyGEN Biotech, Beijing, China) was conducted to evaluate the viability of MG63 cells. Following the same seeding and incubation methods mentioned earlier, all samples were transferred to a new 24-well plate after 1 day of culture, washed twice with PBS, and then stained in the dark at room temperature with 1 mL working solution (containing 5 μL 16 mM propidium iodide and 5 μL 4 mM Calcein-AM in 10 mL PBS) for 30 minutes. After staining, excess working solution was removed from the surfaces by two washes with PBS. Images were acquired with a confocal laser scanning microscope (CLSM, FV1000; Olympus Corporation, Tokyo, Japan).

Proliferation

After culturing for 1, 4, and 7 days, cells on each sample were collected for cell cycle analysis with a KeyGEN DNA Content Quantitation Assay Kit (KeyGEN Biotech). First, cells were washed with PBS and fixed in ice-cold 70% ethanol at 4°C overnight. Then, the fixed cells were washed with PBS and treated with 0.1 mL RNase at 37°C and stained with 0.4 mL propidium iodide solution for 30 minutes at 4°C in the dark. The stained nuclei were analyzed by flow cytometry (BD FACSAria; BD Biosciences, San Jose, CA, USA) to determine the ratio of cells in G_0/G_1, S and G_2/M phases. The proliferation index (PI) was calculated according to Equation 1 as follows:

$$PI = \frac{(G_2/M+S)}{(G_0/G_1+G_2/M+S)}\times 100\%. \quad (1)$$

Real-time quantitative PCR (q-PCR)

After culturing cells for 7 and 14 days, the gene expression of osteogenic differentiation markers (ALP, OC, and Col-I) was determined by q-PCR. Briefly, the total RNA from cells seeded on each sample was extracted using TRIZOL reagent

Table 1 Primers used in q-PCR

Gene	Forward primer sequence (5′–3′)	Reverse primer sequence (5′–3′)
ALP	CCGTGGCAACTCTATCTTTGG	GCCATACAGGATGGCAGTGA
Col-IA I	CCCTGGAAAGAATGGAGATGAT	ACTGAAACCTCTGTGTCCCTTCA
OC	AAGAGACCCAGGCGCTACCT	AACTCGTCACAGTCCCGGATTG
β-Actin	ACCAACTGGGACGACATGGAGAAA	TAGCACAGCCTGGATAGCAACGTA

Abbreviation: q-PCR, quantitative PCR.

(Thermo Fisher Scientific) and treated with recombinant DNase I (RNase-free) to remove genomic DNA contamination (Takara Bio Inc., Tokyo, Japan). The extracted RNA was then reverse transcribed into cDNA using a Super-Script III First-Strand Synthesis System (Thermo Fisher Scientific). q-PCR analysis was performed on an ABI 7500 Real-Time PCR System (Thermo Fisher Scientific) using a SYBR Green PCR Kit (TaKaRa). The PCR conditions were as follows: 95°C for 5 minutes, 40 repetitions at 95°C for 15 seconds, 60°C for 60 seconds, and a final cycle of 5 minutes at 72°C. The primer sequences used in the study are listed in Table 1. β-Actin was used as a housekeeping gene. The ΔΔCt method was applied for measurements of gene expression. Data were normalized to the β-actin mRNA level and converted to a fold change relative to the control (cp-Ti).

Western blot analysis

After culturing cells for 7 and 14 days, total proteins were extracted from cells using RIPA buffer (Beyotime, Guangzhou, China). The protein concentration of the supernatant was assayed with a BCA protein assay kit (Beyotime). Proteins were separated by SDS-PAGE and then transferred onto polyvinylidene fluoride (PVDF) membranes. After blocking for nonspecific binding, the membranes were incubated with primary antibodies (OC, ab13420, 1:500 dilution; Abcam, Cambridge, UK; and Col-I, GTX26308, 1:1,000 dilution; San Antonio, TX, USA) and then incubated with the appropriate horseradish peroxidase-conjugated secondary antibodies. Specific protein bands were visualized using an enhanced chemiluminescence detection system (EMD Millipore, Billerica, MA, USA).

Biocompatibility assays in vivo

Surgical procedures

All experiments were conducted in accordance with Regulations on Laboratory Animal Welfare and Ethical Examination of China Medical University on the protection of animals and approved by the ethics committee of China Medical University. A total of 90 male Sprague Dawley rats (8-week old, weighing 200–250 g; Longyuan Company, Shenyang, China) were used and equally distributed into five groups; each group consisted of six rats for each time point (1, 2, and 4 weeks). Surgeries were performed as previously described.[4] Briefly, following general anesthesia by an intraperitoneal injection of chloral hydrate, the right leg was cleaned with povidone iodine. A medial parapatellar arthrotomy was then performed to expose the intercondylar fossa, which is the deep notch between the medial and lateral femoral condyle (Figure 3A). A 15 mm-long bone tunnel was drilled through the fossa with a 1 mm Kirschner wire into which one sample was inserted (Figure 3B). After rinsing the joint with PBS, the fascia and skin were closed in layers, and a postoperative X-ray (Figure 3C) was performed with a mobile X-ray machine (Mobilett XP Hybrid; Siemens, Berlin, Germany).

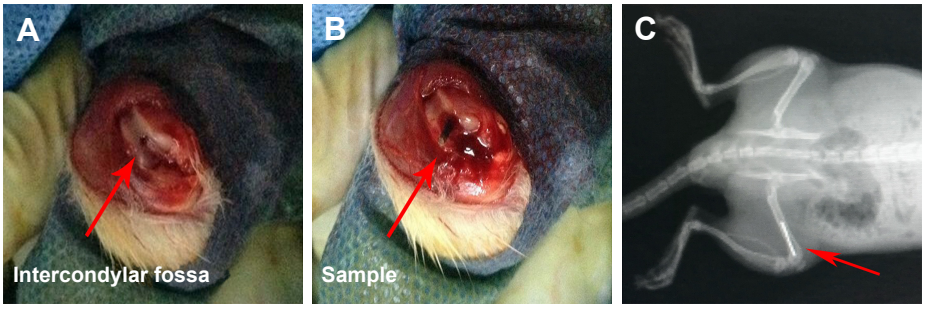

Figure 3 The right femoral condylar insertion model: an implant was inserted into a hole drilled in the intercondylar fossa (**A** and **B**); the postoperative X-ray with the sample in the right femoral condyle (**C**).

Animals were euthanized at 1, 2, and 4 weeks after surgery by the administration of an overdose of chloral hydrate.

Micro-computed tomography (micro-CT)

After euthanasia, the femurs with implants were isolated and fixed in 4% paraformaldehyde and scanned using a Micro X-ray 3D Imaging System (Y.Cheetah, Berlin, Germany), which was set to 90 kV and 50 μA. The scanning resolution was ~9 μm. The region of interest (ROI) was defined as a column (1 mm in height and 1.6 mm in diameter) that was 1.5 mm above the growth plate of the condyles. Four-hundred-fifty projections were reconstructed using a modified parallel Feldkamp algorithm and segmented into binary images (12-bit TIF images). The bone volume per total volume (BV/TV), bone surface per bone volume (BS/BV), mean trabecular thickness (Tb.Th), mean trabecular number (Tb.N), and mean trabecular separation (Tb.Sp) were calculated using a threshold of 200–1,400 for the bone and 1,400–4,095 for the implant via VGStudio MAX software with beam hardening correction, which can decrease metallic artifacts in micro-CT results.[18]

Histological analysis

After decalcification with EDTA, the implants were carefully removed, and the femurs were dehydrated and embedded in paraffin. Tissue sections that were 8 μm in thickness were mounted on glass slides, and HE and Masson's trichrome staining was performed. The bone area ratio (BA), which was calculated as the area percentage of bone tissue to the whole area shown on the image,[19,20] was determined and compared among different groups.

Statistical analysis

One-way ANOVA was used. $P<0.05$ (*) was regarded as significant, and $P<0.01$ (**) was regarded as highly significant. All assays were conducted with triplicate samples. The results were expressed as mean ± SD.

Results and discussion

According to the principle of "race for the surface",[21] the evolution of a biomaterial implant is a competitive race between bacterial colonization and tissue integration. When tissue integration is full and fast, the implant becomes less available and less vulnerable to bacterial colonization.[2] Moreover, we believe that improved osseointegration of implants can promote local immune recovery, which is helpful in the prevention of long-term IRI. Therefore, we advocate that antibacterial biomaterials must have good biocompatibility because it is not only the basis for biosafety but also the key to achieve long-term antibacterial properties.

As shown in Figure 4, we observed cell morphology with SEM. Compared to Ti1%Ag-NT and Ti4%Ag-NT, more

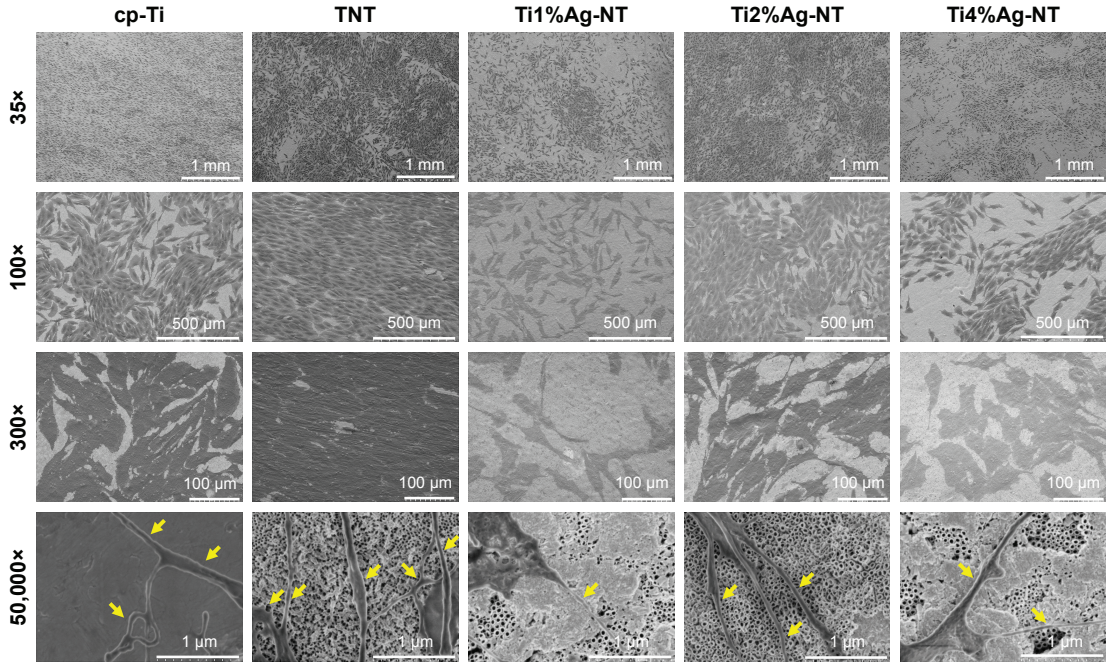

Figure 4 MG63 cell morphology of cp-Ti, TNT, and TiAg-NTs after 1 day of culture.
Note: The arrows indicate the filopodia of MG63 cells on each specimen.
Abbreviations: cp-Ti, commercially pure Ti; TNT, titanium nanotubes; NT, nanotubes.

MG63 cells adhered to the surfaces of cp-Ti, titanium nanotube (TNT), and Ti2%Ag-NT. Furthermore, cells on cp-Ti, TNT, and Ti2%Ag-NT showed a natural spindle shape with round bodies and lamellipodia. The cells spread extensively and showed a clear tendency to clump together and remained in close contact with each other. In contrast, the cell shape on Ti1%Ag-NT and Ti4%Ag-NT was irregular with slim bodies and filopodia, the cellular contact was limited, and there was little tendency to clump together, especially on Ti1%Ag-NT.

Then, we observed cell viability under CLSM. Calcein-AM is a dye that only stains living cells, whereas propidium iodide only stains the nuclei of dead cells. As shown in Figure 5, the largest number of living cells was observed on TNT, followed by cp-Ti, Ti2%Ag-NT, and Ti4%Ag-NT. Ti1%Ag-NT had the smallest number of living cells. This result is consistent with that of SEM described earlier. Furthermore, for propidium iodide staining, only a small amount of dead cells were observed on each sample. There were more dead cells on Ti1%Ag-NT and Ti4%Ag-NT compared to cp-Ti, TNT, and Ti2%Ag-NT; however, these differences were not significant.

After initially adhering to the surface and adapting to the local microenvironment, the cells began to proliferate. The cell cycle propagation of seeded cells was monitored by flow cytometry at days 1, 4, and 7. As shown in Figure 6, the PI of cells on each sample showed no significant differences at day 1. However, the PI of TNT and TiAg-NTs increased rapidly from day 1 to day 4; the PI of TNT was 1.9-fold greater than that of cp-Ti at day 4, and the PI of Ti1%Ag-NT, Ti2%Ag-NT, and Ti4%Ag-NT was 1.4-, 1.6-, and 1.4-fold greater than that of cp-Ti at day 4, respectively. Furthermore, the PI continued to increase until day 7, but no significant differences between each group were observed.

ALP is a marker of cell maturation and early-phase osteogenic differentiation, Col-I is the most abundant component of the extracellular matrix (ECM), and osteocalcin (OC) is a marker of late-phase osteogenic differentiation and bone mineralization.[22] As shown in Figure 7, cells on TNT and Ti2%Ag-NT showed increased ALP expression levels compared to those of cp-Ti at day 7, whereas ALP expression levels of cells on Ti1%Ag-NT and Ti4%Ag-NT were essentially the same as cp-Ti. However, at day 14, there were still differences in the absolute values of ALP expression levels between groups, but no significant differences were observed. In contrast, the expression levels of Col-I and OC between groups were similar at day 7, but the expression levels increased rapidly from day 7 to day 14, and we observed that cells on TNT and Ti2%Ag-NT exhibited higher gene expression levels compared to those of cells on cp-Ti at day 14, whereas cells on Ti1%Ag-NT and Ti4%Ag-NT showed significantly lower gene expression levels. Consistent with the results of q-PCR, as shown in Figure 8, no significant differences were observed in the protein expression levels of Col-I and OC at day 7, but they were both significantly enhanced by TNT at day 14 ($P<0.01$), and comparable protein expression levels were observed for cells

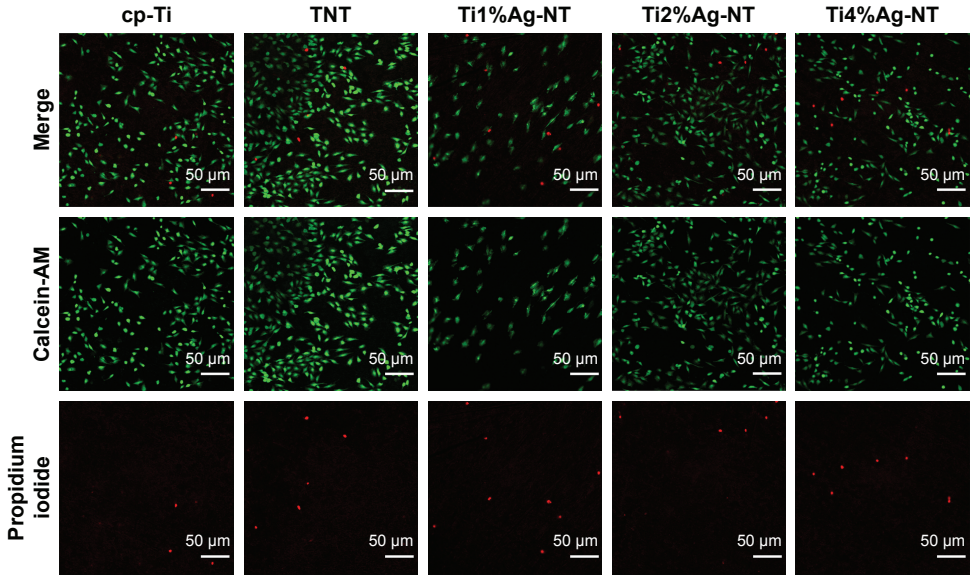

Figure 5 CLSM images of MG63 cells seeded on cp-Ti, TNT, and TiAg-NTs after 1 day of culture.
Note: Green fluorescence indicates living cells, and red fluorescence indicates dead cells.
Abbreviations: CLSM, confocal laser scanning microscope; cp-Ti, commercially pure Ti; NT, nanotubes; TNT, titanium nanotubes.

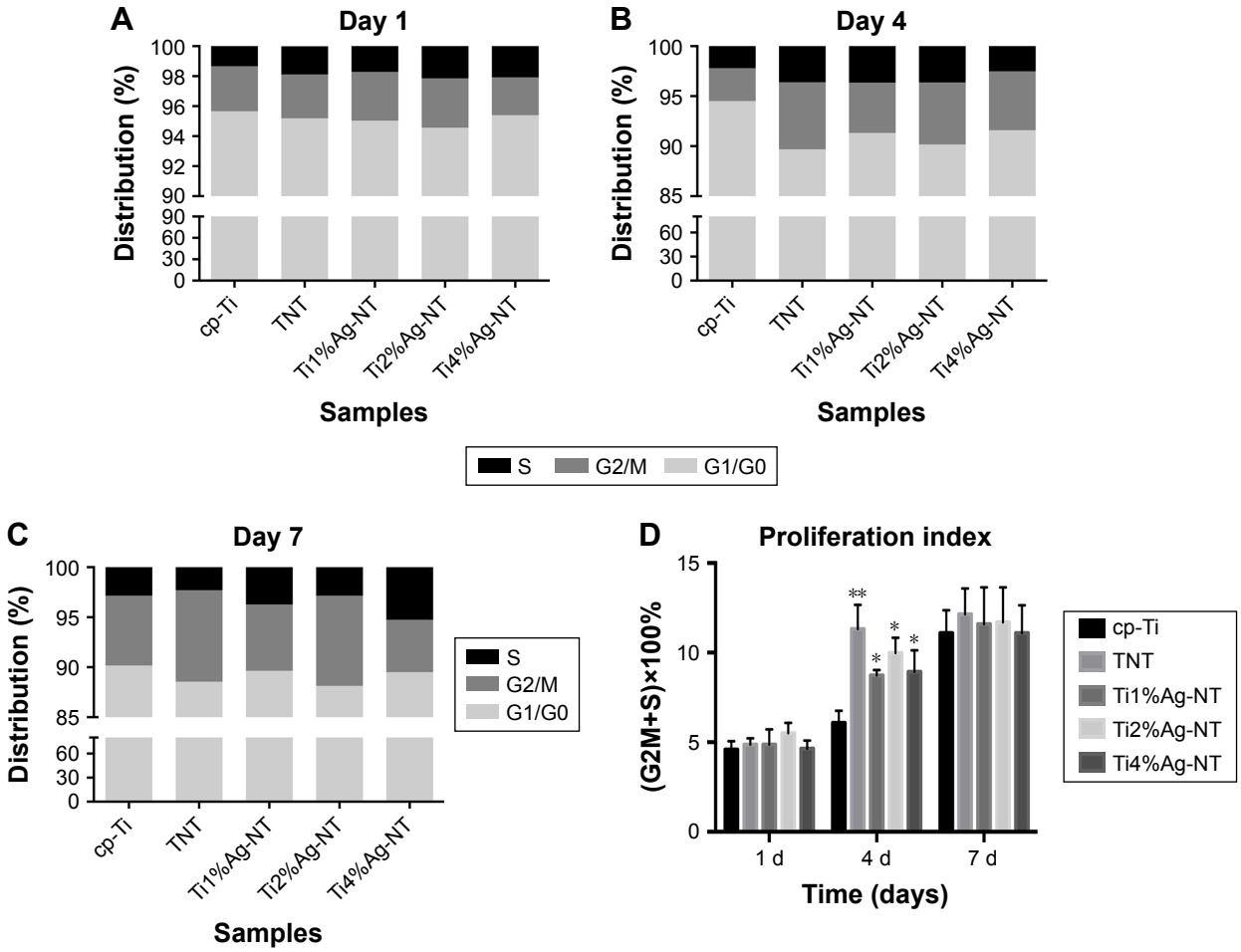

Figure 6 Histographic representations of cell cycle distribution (**A**–**C**) and the proliferation index of cells on each substrate (**D**) at days 1, 4, and 7.
Note: All values are reported as the mean ± SD (n=3). *$P<0.05$ and **$P<0.01$.
Abbreviations: cp-Ti, commercially pure Ti; d, days; NT, nanotubes; TNT, titanium nanotubes.

on Ti2%Ag-NT compared to cells on cp-Ti, whereas cells on Ti1%Ag-NT and Ti4%Ag-NT exhibited significantly lower protein expression levels compared to those for cells on the control sample.

It was observed from the abovementioned results that the cytocompatibility of Ti2%Ag-NT was satisfactory, whereas Ti1%Ag-NT and Ti4%Ag-NT exhibited noticeable cytotoxicity compared with cp-Ti. Therefore, we speculated whether the in vivo biocompatibility of TiAg-NTs exhibited similar trends. To investigate the in vivo biocompatibility, we performed two experiments using the femoral condyle insertion model, which included micro-CT and histological analysis. Micro-CT can quantitatively analyze cancellous bone in a preset ROI area around the implant and evaluate implant osseointegration. We obtained five different types of results from the micro-CT data, and BV/TV is the most direct parameter for evaluating the amount of cancellous bone around the implant. As shown in Figures 9 and 10, TNT showed the best osseointegration at all time points. The amount of cancellous bone around Ti2%Ag-NT was significantly greater than that of cp-Ti at week 2, whereas no significant differences were observed at the other time points. Furthermore, the BV/TV values of Ti1%Ag-NT and Ti4%Ag-NT were less than those of cp-Ti to varying degrees. Consistently, as shown in Figures 11 and 12, the BA value of TNT was always the greatest in the histological staining. The BA value of Ti2%Ag-NT was greater than that of cp-Ti, although there was no significant difference. The amounts of cancellous bone around Ti1%Ag-NT and Ti4%Ag-NT were less than that of cp-Ti.

In addition, from week 1 to week 4, the amount of cancellous bone (BV/TV) around all implants continued to decrease, which was also confirmed by histological staining (BA value). We speculate that this was not an anomaly caused by the materials. Instead, we hypothesize that it was the result of the normal healing process between the implant

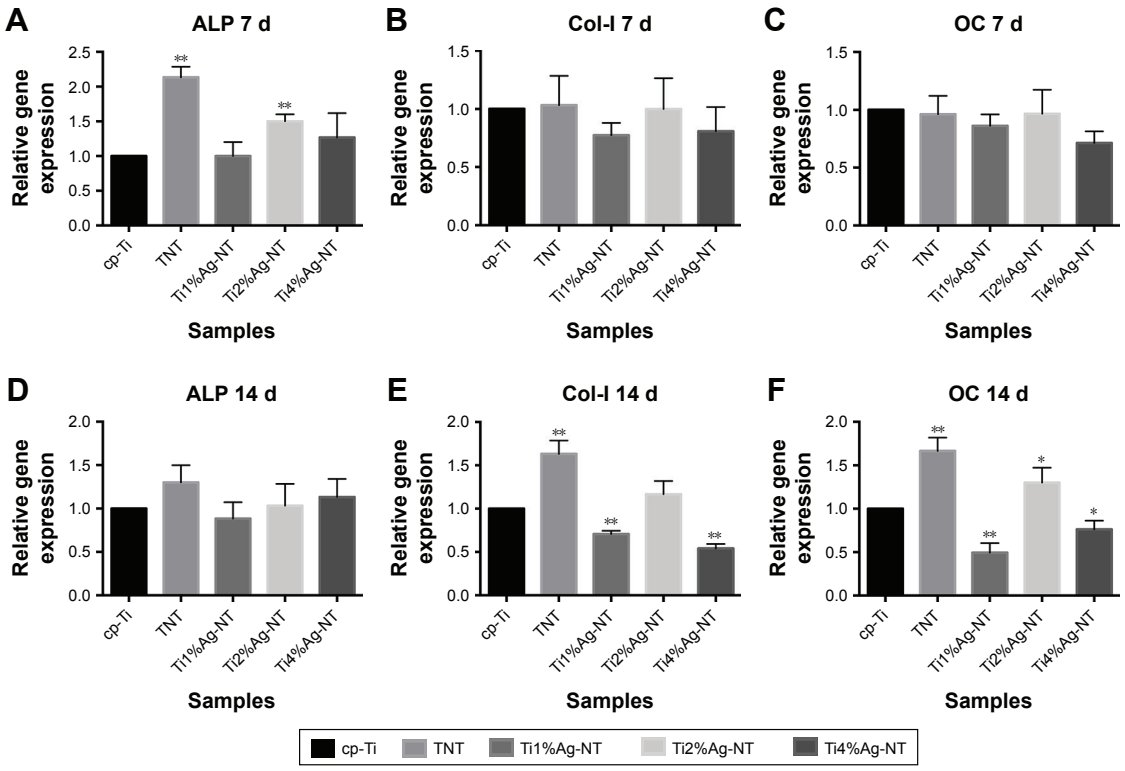

Figure 7 Relative gene expression levels of cells on each sample at days 7 and 14: (**A** and **D**) ALP, (**B** and **E**) Col-I, and (**C** and **F**) OC gene expression levels.
Notes: All values are reported as mean ± SD (n=3). Data were normalized to the β-actin mRNA expression level and converted to the fold change relative to cells on the control sample (cp-Ti). *$P<0.05$ and **$P<0.01$.
Abbreviations: Col-I, collagen-I; cp-Ti, commercially pure Ti; d, days; NT, nanotubes; OC, osteocalcin; TNT, titanium nanotubes.

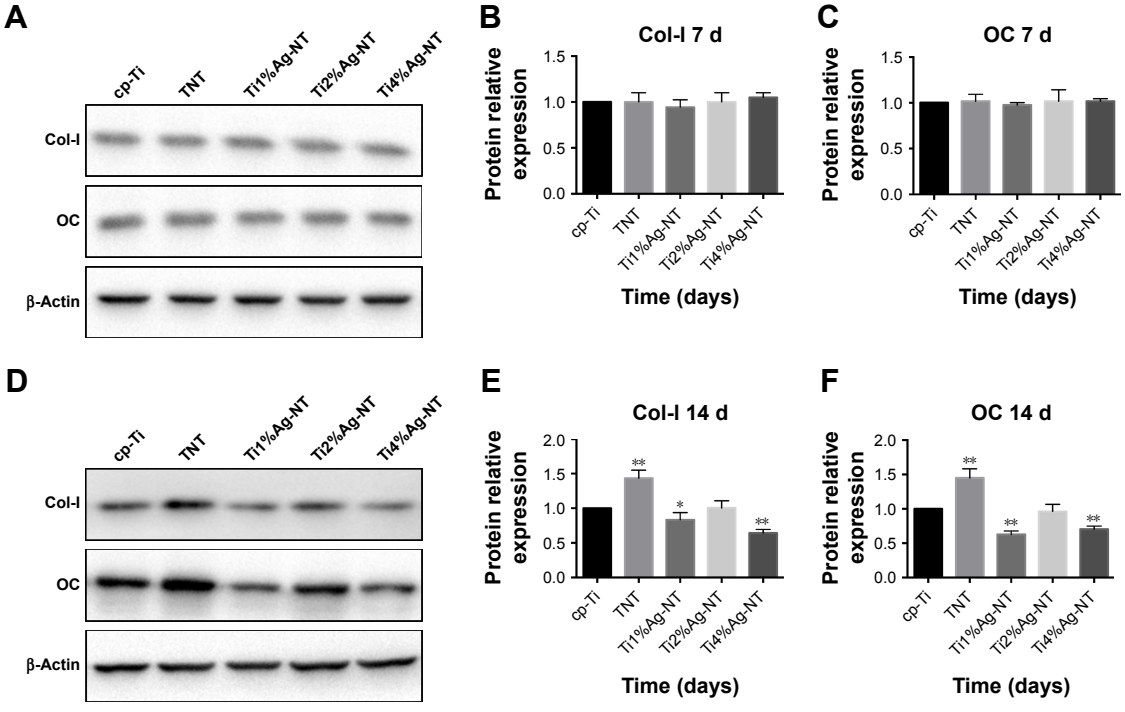

Figure 8 Western blot analysis of Col-I and OC protein expression levels at days 7 and 14: (**A**–**C**) Col-I and OC expression at day 7; (**D**–**F**) Col-I and OC expression at day 14.
Notes: Data were normalized to the β-actin protein expression level and converted to the fold change relative to cells on the control sample (cp-Ti). *$P<0.05$ and **$P<0.01$.
Abbreviations: Col-I, collagen-I; cp-Ti, commercially pure Ti; NT, nanotubes; OC, osteocalcin; TNT, titanium nanotubes.

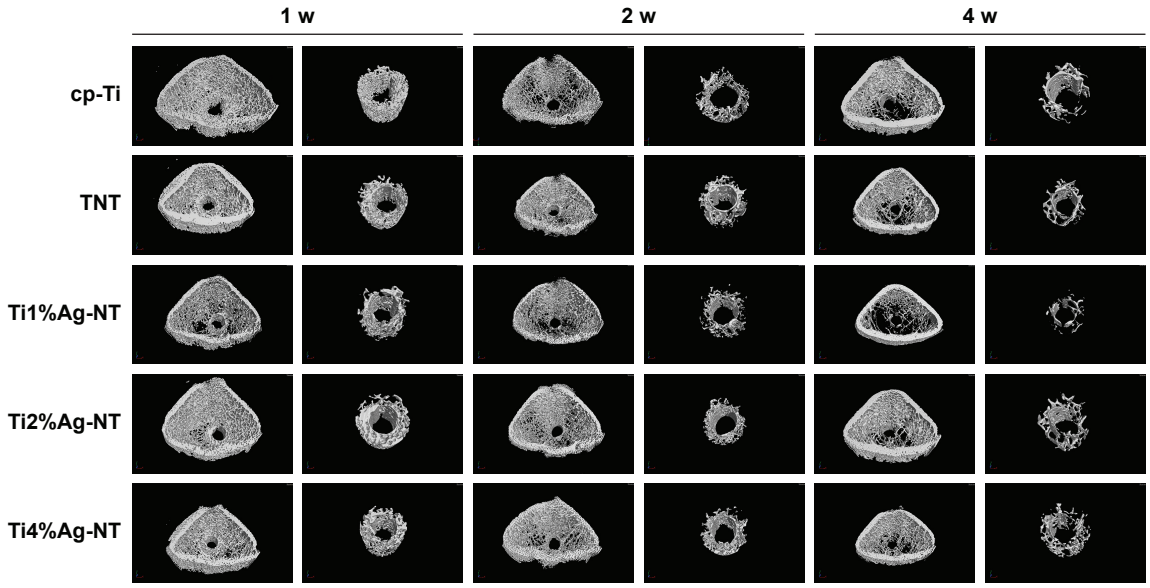

Figure 9 Representative 3D micro-CT images of the femoral condyle at 1, 2, and 4 weeks after sample implantation.
Abbreviations: cp-Ti, commercially pure Ti; NT, nanotubes; TNT, titanium nanotubes; w, weeks.

and bone tissue within this femoral condylar insertion model. When drilling the hole with Kirschner wire, it squeezed the cancellous bone to the periphery; therefore, the pressure caused an increase in the amount of cancellous bone around the bone tunnel and the highest BV/TV value at week 1. Then, as the healing between the implant and the cancellous bone proceeded and entered into the remodeling phase, the cancellous bone began to restore its original appearance, resulting in a continuous decrease in BV/TV. However, this downward trend should not last long, and we speculate that

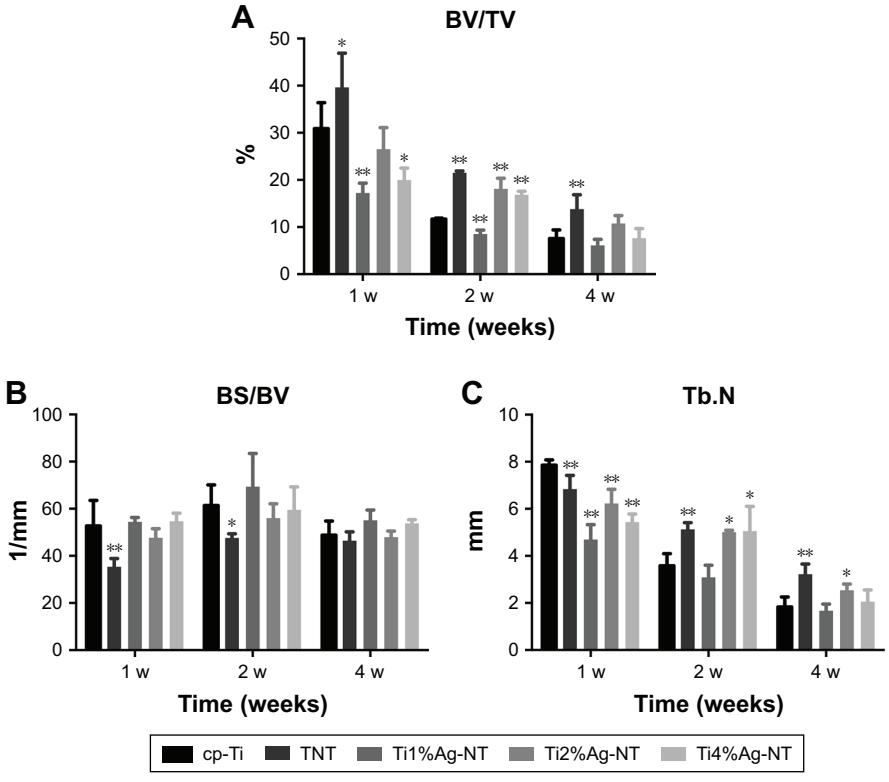

Figure 10 (*Continued*)

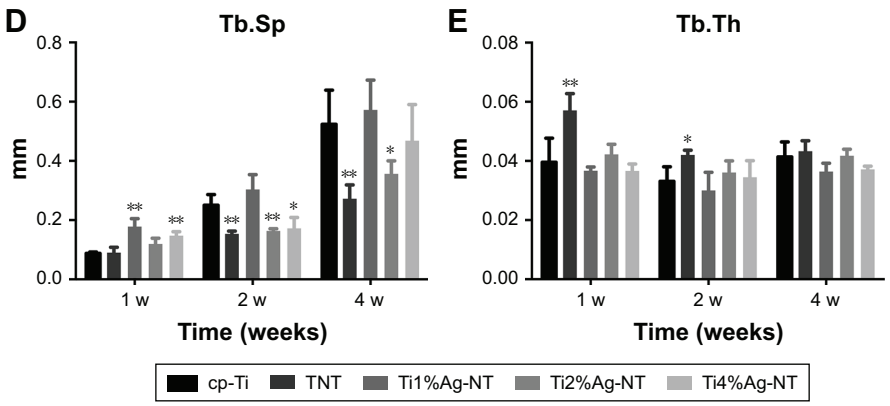

Figure 10 The (**A**) BV/TV, (**B**) BS/BV, (**C**) Tb.N, (**D**) Tb.Sp, and (**E**) Tb.Th in the rat femoral condylar insertion model after samples were implanted for 1, 2, and 4 weeks.
Notes: All values are reported as mean ± SD (n=3). *$P<0.05$ and **$P<0.01$.
Abbreviations: BS/BV, bone surface per bone volume; BV/TV, bone volume per total volume; cp-Ti, commercially pure Ti; NT, nanotubes; Tb.N, mean trabecular number; Tb.Sp, mean trabecular separation; Tb.Th, mean trabecular thickness; TNT, titanium nanotubes; w, weeks.

it reaches a plateau with a stable cancellous bone volume at the end of the remodeling phase. However, the observation time of this experiment was only for 4 weeks after surgery, and the healing process was still in the remodeling phase; therefore, the plateau of the BV/TV value was not observed. We will extend the observation time in subsequent experiments to test this hypothesis.

As discussed in our previous study, the biocompatibility of Ti2%Ag-NT was essentially determined by two factors as follows: the positive effect of the nanotube coating and the low toxicity of 2% Ag content.[12] The enhanced biocompatibility provided by nanotube coatings has been extensively reported;[7,10,23] however, for Ag-containing biomaterials, it is uncertain if 2% Ag content is optimal for low toxicity.

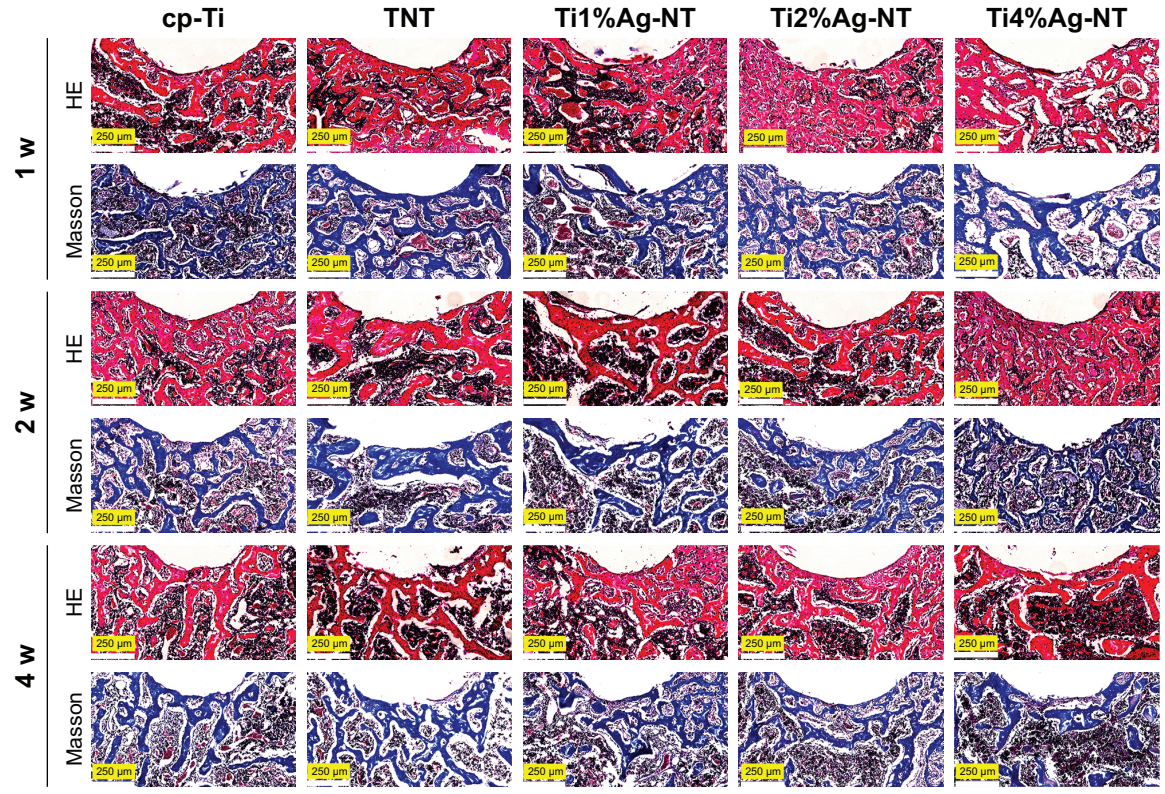

Figure 11 Histological sections of bone formation around implanted samples at 1, 2, and 4 weeks after sample implantation.
Abbreviations: cp-Ti, commercially pure Ti; NT, nanotubes; TNT, titanium nanotubes; w, weeks.

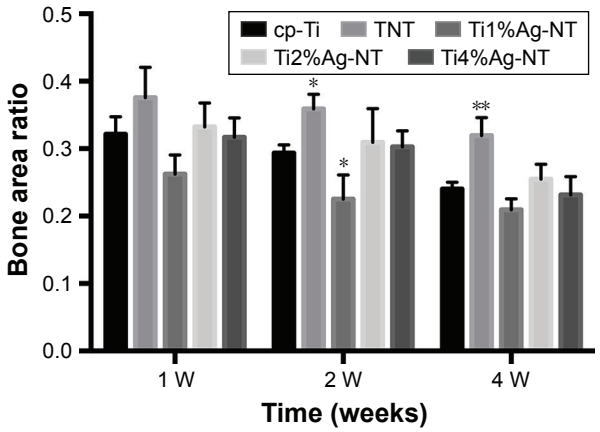

Figure 12 The bone area ratio of each sample at 1, 2, and 4 weeks after sample implantation. All values are reported as mean ± SD (n=3). *$P<0.05$ and **$P<0.01$.
Abbreviations: cp-Ti, commercially pure Ti; NT, nanotubes; TNT, titanium nanotubes; w, weeks.

Consistent with this study, Jamuna-Thevi et al[24] demonstrated that 2 wt% Ag-TiO_2 exhibited the greatest cell viability after fibroblasts were cultured in the extracts for 6 hours compared to those of cells cultured in 1, 3, and 4 wt% Ag-TiO_2. Jähn et al[25] proposed that Mg/2% Ag implants could be promising for the intramedullary fixation of long-bone fractures. However, in research conducted by Zheng et al,[26] 1.4 wt% Ag was precipitated within a Ti–Ni alloy matrix to obtain a new shape memory alloy with combined antibacterial activity and biocompatibility. In another study, 2.5 wt% Ag was used to develop a bioactive, corrosion resistant, and antibacterial hydroxyapatite/titania composite coating.[27] Based on these results, it is difficult to reach a consensus regarding the optimal content of Ag, but it is likely to obtain a good result when the Ag content is approximately 2%.

In this study, the remaining 96% of the Ag content range was not investigated, which raises questions regarding the effects of increasing Ag contents. Huang et al[28] showed that a TaN-21.4% Ag film exhibited a greater cell viability than those of TaN-14.9% Ag and TaN-17.5% Ag films, and this was a positive dose-dependent trend. In contrast, a negative dose-dependent trend was observed because the bioactivity was reduced when the Ag content was increased in TiO_2-Ag.[29] In this study, the influence of Ag content on biocompatibility was not dose dependent. The biocompatibility of Ti2%Ag-NT was significantly greater compared to those of both Ti1%Ag-NT and Ti4%Ag-NT. Similarly, Kang et al[30] showed that Ti2%Ag had improved osteoblast viability than those of Ti1%Ag and Ti4%Ag. Chang et al[31] showed that the cytotoxicity of ZrNO-5%Ag was greater than those of ZrNO-2%Ag and ZrNO-12%Ag.

Therefore, questions remain regarding how much Ag content is less toxic and the relationship between the amount of Ag and the biocompatibility of the biomaterial. Through the above discussion, we are temporarily unable to provide a definitive answer to these two questions. The influence of a biomaterial on the cell or host is complex, and there are many factors involved. In this study, the factors that influenced the behavior of TiAg-NTs mainly included a biochemical factor, which includes the effect of Ag ions and incorporation of fluoride species when fabricating nanotubes; a structural factor, which is associated with the nanotopography of nanotube coatings; and a mechanical factor, which refers to the stiffness and Young's modulus of different substrates.[1] For different Ag-containing biomaterials, they differ in the aforementioned three key factors, which is why we are unable to draw conclusions about the optimal Ag content and its impact.

Conclusion

Nanotubular coatings were fabricated on Ti–Ag sintered alloy samples (1, 2, and 4 wt% Ag). Ti2%Ag-NT was as good as cp-Ti in terms of cytocompatibility in vitro and osseointegration in vivo, and Ti2%Ag-NT is thus a potential biomaterial for orthopedics. Ti4%Ag-NT was less biocompatible than cp-Ti, and Ti1%Ag-NT was the worst among all the samples.

Acknowledgments

This work was supported by the Special Research Foundation of the Health and Family Planning Commission of Liaoning Province (LNCCC-A03-2014), the National Natural Science Foundation of China (51801027, 81671811, 81501857, 81572108, and 81772339), Post Doctoral Foundation of China (2017M621366), the Science and Technology Project of Shenyang city (17-230-9-09), National Key R&D Program of China (2016YFC1100300, 2017YFC0840100, and 2017YFC0840106), the Key Clinical Medicine Center of Shanghai (2017ZZ01006), Sanming Project of Medicine in Shenzhen (SZSM201612078), Shanghai Rising-Star Project (18QB1400500), and the Introduction Project of Clinical Medicine Expert Team for Suzhou (SZYJTD201714). This manuscript was edited for English language by American Journal Experts (AJE).

Disclosure

The authors report no conflicts of interest in this work.

References

1. Ferraris S, Spriano S. Antibacterial titanium surfaces for medical implants. *Mater Sci Eng C*. 2016;61:965–978.

2. Cheng H, Xiong W, Fang Z, et al. Strontium (Sr) and silver (Ag) loaded nanotubular structures with combined osteoinductive and antimicrobial activities. *Acta Biomater*. 2016;31:388–400.
3. Crespo-Monteiro N, Destouches N, Bois L, Chassagneux F, Reynaud S, Fournel T. Reversible and irreversible laser microinscription on silver-containing mesoporous titania films. *Adv Mater*. 2010;22(29): 3166–3170.
4. Zhang H, Sun Y, Tian A, et al. Improved antibacterial activity and biocompatibility on vancomycin-loaded TiO2 nanotubes: in vivo and in vitro studies. *Int J Nanomedicine*. 2013;8:4379–4389.
5. Lei Z, Zhang H, Zhang E, You J, Ma X, Bai X. Antibacterial activities and biocompatibilities of Ti-Ag alloys prepared by spark plasma sintering and acid etching. *Mater Sci Eng C Mater Biol Appl*. 2018;92: 121–131.
6. Shivaram A, Bose S, Bandyopadhyay A. Understanding long-term silver release from surface modified porous titanium implants. *Acta Biomater*. 2017;58:550–560.
7. Gulati K, Maher S, Findlay DM, Losic D. Titania nanotubes for orchestrating osteogenesis at the bone-implant interface. *Nanomedicine*. 2016;11(14):1847–1864.
8. Crawford GA, Chawla N, das K, Bose S, Bandyopadhyay A. Microstructure and deformation behavior of biocompatible TiO2 nanotubes on titanium substrate. *Acta Biomater*. 2007;3(3):359–367.
9. Su EP, Justin DF, Pratt CR, et al. Effects of titanium nanotubes on the osseointegration, cell differentiation, mineralisation and antibacterial properties of orthopaedic implant surfaces. *Bone Joint J*. 2018; 100-B(1 Supple A):9–16.
10. Brammer KS, Frandsen CJ, Jin S. TiO2 nanotubes for bone regeneration. *Trends Biotechnol*. 2012;30(6):315–322.
11. Tian A, Qin X, Wu A, et al. Nanoscale TiO2 nanotubes govern the biological behavior of human glioma and osteosarcoma cells. *Int J Nanomedicine*. 2015;10:2423–2439.
12. Liu X, Tian A, You J, et al. Antibacterial abilities and biocompatibilities of Ti-Ag alloys with nanotubular coatings. *Int J Nanomedicine*. 2016;11:5743–5755.
13. Xie X, Mao C, Liu X, et al. Tuning the bandgap of photo-sensitive polydopamine/Ag_3PO_4/Graphene oxide coating for rapid, noninvasive disinfection of implants. *ACS Cent Sci*. 2018;4(6):724–738.
14. Mao C, Xiang Y, Liu X, et al. Photo-inspired antibacterial activity and wound healing acceleration by hydrogel embedded with Ag/Ag@AgCl/ZnO nanostructures. *ACS Nano*. 2017;11(9):9010–9021.
15. Jin C, Liu X, Tan L, et al. Ag/AgBr-loaded mesoporous silica for rapid sterilization and promotion of wound healing. *Biomater Sci*. 2018;6(7): 1735–1744.
16. Xiang Y, Li J, Liu X, et al. Construction of poly(lactic-co-glycolic acid)/ZnO nanorods/Ag nanoparticles hybrid coating on Ti implants for enhanced antibacterial activity and biocompatibility. *Mater Sci Eng C Mater Biol Appl*. 2017;79:629–637.
17. Zheng Y, Li J, Liu X, Sun J. Antimicrobial and osteogenic effect of Ag-implanted titanium with a nanostructured surface. *Int J Nanomedicine*. 2012;7:875–884.
18. Li Y, Yang W, Li X, et al. Improving osteointegration and osteogenesis of three-dimensional porous Ti6Al4V scaffolds by polydopamine-assisted biomimetic hydroxyapatite coating. *ACS Appl Mater Interfaces*. 2015;7(10):5715–5724.
19. Cheng H, Li Y, Huo K, Gao B, Xiong W. Long-lasting *in vivo* and *in vitro* antibacterial ability of nanostructured titania coating incorporated with silver nanoparticles. *J Biomed Mater Res A*. 2014;102(10):3488–3499.
20. Xu B, Zhang J, Brewer E, et al. Osterix enhances BMSC-associated osseointegration of implants. *J Dent Res*. 2009;88(11):1003–1007.
21. Gristina AG. Biomaterial-centered infection: microbial adhesion versus tissue integration. *Science*. 1987;237(4822):1588–1595.
22. Santana-Melo GF, Rodrigues BVM, da Silva E, et al. Electrospun ultra-thin PBAT/nHAp fibers influenced the in vitro and in vivo osteogenesis and improved the mechanical properties of neoformed bone. *Colloids Surf B: Biointerfaces*. 2017;155:544–552.
23. Park J, Bauer S, Schlegel KA, Neukam FW, von der Mark K, Schmuki P. TiO2 nanotube surfaces: 15 nm – an optimal length scale of surface topography for cell adhesion and differentiation. *Small*. 2009;5(6): 666–671.
24. Jamuna-Thevi K, Bakar SA, Ibrahim S, Shahab N, Toff MRM. Quantification of silver ion release, in vitro cytotoxicity and antibacterial properties of nanostuctured Ag doped TiO2 coatings on stainless steel deposited by RF magnetron sputtering. *Vacuum*. 2011;86(3):235–241.
25. Jähn K, Saito H, Taipaleenmäki H, et al. Intramedullary Mg2Ag nails augment callus formation during fracture healing in mice. *Acta Biomater*. 2016;36:350–360.
26. Zheng YF, Zhang BB, Wang BL, et al. Introduction of antibacterial function into biomedical TiNi shape memory alloy by the addition of element Ag. *Acta Biomater*. 2011;7(6):2758–2767.
27. Venkateswarlu K, Rameshbabu N, Chandra Bose A, et al. Fabrication of corrosion resistant, bioactive and antibacterial silver substituted hydroxyapatite/titania composite coating on Cp Ti. *Ceram Int*. 2012;38(1): 731–740.
28. Huang H-L, Chang Y-Y, Lai M-C, Lin C-R, Lai C-H, Shieh T-M. Antibacterial TaN-Ag coatings on titanium dental implants. *Surf Coat Tech*. 2010;205(5):1636–1641.
29. Santillán MJ, Quaranta NE, Boccaccini AR. Titania and titania–silver nanocomposite coatings grown by electrophoretic deposition from aqueous suspensions. *Surf Coat Tech*. 2010;205(7):2562–2571.
30. Kang M-K, Moon S-K, Kwon J-S, Kim K-M, Kim K-N. Antibacterial effect of sand blasted, large-grit, acid-etched treated Ti–Ag alloys. *Mater Res Bull*. 2012;47(10):2952–2955.
31. Chang Y-Y, Huang H-L, Chen Y-C, Weng J-C, Lai C-H. Characterization and antibacterial performance of ZrNO–Ag coatings. *Surf Coat Techn*. 2013;231:224–228.